

## Probing $\text{La}_{0.7}\text{Sr}_{0.3}\text{MnO}_3$ multilayers via spin wave resonances

Rhet Magaraggia,<sup>1,\*</sup> Michael Hambe,<sup>2</sup> Mikhail Kostylev,<sup>1</sup> Valanoor Nagarajan,<sup>2</sup> and R. L. Stamps<sup>1,3</sup>

<sup>1</sup>*School of Physics, University of Western Australia, 35 Stirling Highway, Crawley, Western Australia 6009, Perth, Australia*

<sup>2</sup>*School of Materials Science and Engineering, University of New South Wales, New South Wales 2052, Sydney, Australia*

<sup>3</sup>*SUPA, School of Physics and Astronomy, University of Glasgow, Glasgow G12 8QQ, United Kingdom*

(Received 20 December 2010; revised manuscript received 11 August 2011; published 26 September 2011)

Epitaxial  $\text{La}_{0.7}\text{Sr}_{0.3}\text{MnO}_3/\text{BiFeO}_3$  and  $\text{La}_{0.7}\text{Sr}_{0.3}\text{MnO}_3/\text{PbZr}_{20}\text{Ti}_{80}\text{O}_3$  heterostructures were grown on  $\text{SrTiO}_3$  substrates via pulsed laser deposition. We employed spin wave resonances to study the interfacial properties of the ferromagnetic  $\text{La}_{0.7}\text{Sr}_{0.3}\text{MnO}_3$  thin film. We found that the addition of the  $\text{BiFeO}_3$  or  $\text{PbZr}_{20}\text{Ti}_{80}\text{O}_3$  ferroelectric capping layers may cause out-of-plane surface pinning of  $\text{La}_{0.7}\text{Sr}_{0.3}\text{MnO}_3$ . We are able to place limits on the exchange constant  $D$  of  $\text{La}_{0.7}\text{Sr}_{0.3}\text{MnO}_3$  grown on these substrates and confirm the presence of uniaxial and biaxial anisotropies induced by the  $\text{SrTiO}_3$  substrate.

DOI: [10.1103/PhysRevB.84.104441](https://doi.org/10.1103/PhysRevB.84.104441)

PACS number(s): 75.70.Cn, 75.30.Gw, 75.85.+t, 75.30.Ds

### I. INTRODUCTION

The promise of electrically and magnetically tunable tunnel junctions for use in both spin valves and four-state memory devices<sup>1–3</sup> is an exciting prospect.  $\text{La}_{1-x}\text{Sr}_x\text{MnO}_3/\text{BiFeO}_3$  (LSMO/BFO) multilayers have been proposed for use in spin valve devices as LSMO has demonstrated good spin-filtering properties<sup>4</sup> and BFO is a room-temperature multiferroic which could, in principle, provide an electrically tunable exchange-biased film.<sup>5–7</sup> Furthermore, both of these perovskite materials have small lattice mismatches when grown on a suitable substrate. Practically, it is important to understand how the magnetization of a LSMO film is affected when epitaxially joined to a ferroelectric material. Enhancement of uniaxial anisotropies, development of unidirectional anisotropies, surface pinning from the interface, and changes to other micromagnetic parameters are all important characteristics with respect to tunnel junction performance. Though most of these properties have been explored in single-layer LSMOs,<sup>8–16</sup> the effects of ferroelectric overlayers can be important and have begun to be studied.<sup>17,18</sup> In this paper, we examine the pinning of dynamic magnetization using spin wave measurements. A result is our measurement of the spin wave exchange constant  $D$ . To the best of the authors' knowledge, only four other measurements of  $D$  have been carried out so far,<sup>11,19–21</sup> and there has been only one study which utilizes standing spin wave modes for the determination of  $D$ .<sup>11</sup> We also use standing spin wave resonances to measure anisotropies caused by both the ferroelectric overlayer and growth of LSMO on a single-crystal substrate.

### II. STANDING SPIN WAVE MODES

A powerful technique to probe magnetic conditions at buried interfaces involves using spin wave resonances.<sup>22–28</sup> The structure of standing spin wave modes contains detailed information about bulk magnetic properties, such as the gyromagnetic ratio  $\gamma$  and exchange constant  $D$ , and also provides information about interfacial pinning of the magnetization vector.

The ferromagnetic resonance frequency for out-of-plane magnetized thin films is

$$\frac{\omega}{\gamma} = \mu_0 H_{\text{eff}} + \mu_0 H_f, \quad (1)$$

where  $\mu_0 H_{\text{eff}} = -\mu_0 M_S + \mu_0 H_{\text{oop}} + Dk_{\text{oop}}^2$ ,  $\omega$  is the precession frequency,  $\gamma$  is the gyromagnetic ratio,  $H_f$  is the externally applied field,  $\mu_0 M_S$  is the demagnetizing field due to the out-of-plane alignment of spins,  $H_{\text{oop}}$  is any bulk out-of-plane anisotropy field, and  $Dk_{\text{oop}}^2$  is the exchange energy of the standing spin wave mode. Measurement of multiple modes allows determination of  $\gamma$  and  $H_{\text{eff}}$ . Separation of  $-\mu_0 M_S + \mu_0 H_A$  and  $Dk_{\text{oop}}^2$  is possible when the fundamental mode resonance frequency (FMR mode) and the first exchange mode (FEX mode) are measured. Due to the shorter wavelength and much higher energy density of the FEX mode, any changes in wavelength due to surface pinning strongly affect the frequency gap between the FEX and FMR modes. Subtraction of the effective field data of the FEX mode  $H_{\text{eff}}$  (FEX) from the FMR mode  $H_{\text{eff}}$  (FMR) gives us a measure of the strength of pinning and the exchange constant.

Angular dependence of spin wave frequencies for in-plane magnetization can be used to measure magnetocrystalline anisotropies. The Kittel formula describing resonance conditions for the magnetization oriented in-plane is<sup>25</sup>

$$\left(\frac{\omega}{\gamma}\right)^2 = [\mu_0 H_f(\theta) + \mu_0 M_S - \mu_0 H_{\text{oop}} + \mu_0 H_{\text{ip}}(\theta) + Dk_{\text{ip}}^2(\theta)][\mu_0 H_f(\theta) + \mu_0 H_{\text{ip}}(\theta) + Dk_{\text{ip}}^2(\theta)]. \quad (2)$$

Here,  $H_{\text{ip}}$  is the in-plane bulk anisotropy, and  $k_{\text{ip}}^2$  refers to the wave vector of the standing wave modes with magnetization aligned in plane. We distinguish  $k_{\text{ip}}^2$  from  $k_{\text{oop}}^2$ , which need not in general be the same, depending upon pinning conditions at the film interface. Also included is an angular dependence. The angle  $\theta$  denotes the magnetization direction with respect to some arbitrary in-plane film direction. By rotating the film in-plane with respect to the applied field and measuring the resonance conditions for each film orientation, the angular variation of pinning and bulk anisotropies may be determined.

The paper is structured as follows. We first describe sample growth and characterization and the ferromagnetic resonance experiment. FMR results are presented along with a discussion of bulk and surface anisotropies. We conclude with results for the exchange constant  $D$  of  $\text{La}_{1-x}\text{Sr}_x\text{MnO}_3$  films.

### III. SAMPLE GROWTH AND CHARACTERIZATION

A series of films containing epitaxial  $\text{La}_{0.7}\text{Sr}_{0.3}\text{MnO}_3$  (LSMO) were grown on single-crystal (100)-oriented  $\text{SrTiO}_3$  (STO) substrates with the addition of either an epitaxial  $\text{BiFeO}_3$  (BFO) or a  $\text{PbZr}_{20}\text{Ti}_{80}\text{O}_3$  (PZT) capping layer. All films were grown via pulsed laser deposition (PLD) with a KrF excimer laser at 248 nm with a laser fluency of  $\sim 2 \text{ J cm}^{-2}$ . The STO substrates were sourced from Shinkosha Co., Ltd., (Japan) with less than a  $0.3^\circ$  miscut and arrived pre-etched to provide a  $\text{TiO}_2$ -terminated surface. All substrates were sonicated in isopropyl alcohol to remove organic contaminants before use. The deposition chamber base pressure was better than  $5.0 \times 10^{-7}$  Torr before the sample was heated to deposition temperature and partial oxygen pressure was introduced. LSMO films were deposited at  $700^\circ\text{C}$  with an oxygen partial pressure of 100 mT, repetition rate of 10 Hz, and laser fluence of  $1.8 \text{ J cm}^{-2}$  and were cooled under 300 Torr  $\text{O}_2$  at  $5^\circ\text{C}$  per minute. BFO films were deposited at  $700^\circ\text{C}$  with an oxygen partial pressure of 5 mT, repetition rate of 20 Hz, and laser fluence of  $1.6 \text{ J cm}^{-2}$  and were cooled under 220 Torr  $\text{O}_2$  at  $5^\circ\text{C}$  per minute. PZT films were deposited at  $550^\circ\text{C}$  with an oxygen partial pressure of 100 mT, repetition rate of 3 Hz, and laser fluence of  $1.6 \text{ J cm}^{-2}$  and were cooled under 700 Torr  $\text{O}_2$  at  $5^\circ\text{C}$  per minute. The growth rates of LSMO, BFO, and PZT were  $\sim 0.002 \text{ nm/pulse}$ ,  $\sim 0.004 \text{ nm/pulse}$ , and  $\sim 0.002 \text{ nm/pulse}$ , respectively. LSMO and BFO phase purities were confirmed via standard x-ray diffraction on a Philips Xpert Pro MRD system. An example is shown in Fig. 1.

The LSMO thickness was calibrated via x-ray reflectivity measurements on a Philips Xpert Pro MRD system. The BFO thickness was calibrated via TEM analysis as published in Hambe *et al.*'s work.<sup>29</sup> Our samples exhibit low surface

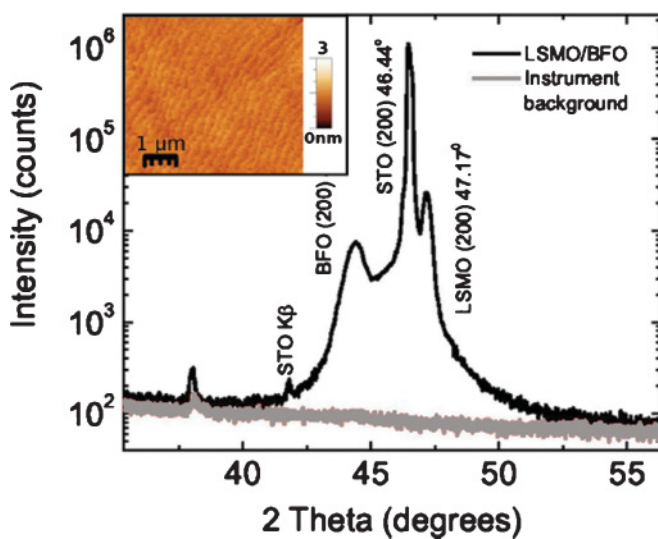


FIG. 1. (Color online) A characteristic XRD image of the LSMO (55 nm) / BFO (18 nm) film showing excellent phase purity. The inset demonstrates the step structure imaged via AFM, which originates on the surface of the of the LSMO (38.9 nm) sample due to epitaxial growth on top of the stepped substrate.

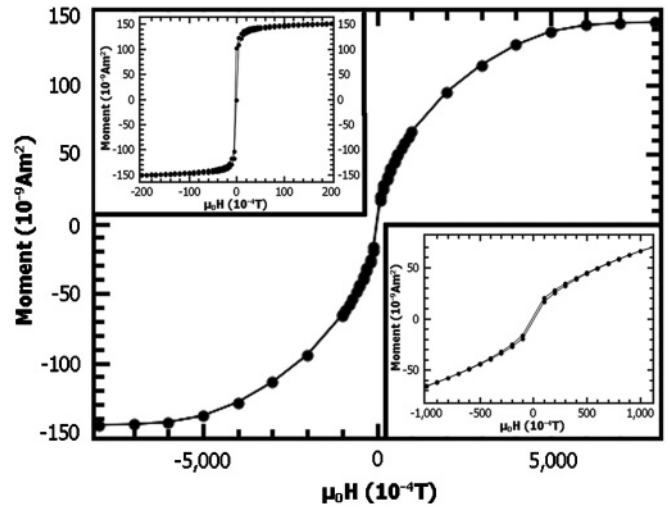


FIG. 2. SQUID data taken for a 38.9-nm-thick LSMO film at room temperature with the field applied out of the film plane. The bottom right inset displays a zoomed in view of the out-of-plane hysteresis loop, and the top left inset displays the SQUID hysteresis with the field applied in the plane of the film.

roughness, less than  $2.6 \text{ \AA}$  root mean square, indicating smooth growth as shown in Fig. 1.

A step pattern is seen which exists in the underlying STO substrates and is preserved throughout the LSMO epitaxial growth. In-plane and out-of-plane superconducting quantum interference device (SQUID) magnetometry was performed, and from these data (seen in Fig. 2),  $\mu_0 M_S - \mu_0 H_{\text{oop}}$  was determined to be  $\sim 0.5 \pm 0.05 \text{ T}$ .

### IV. FERROMAGNETIC RESONANCE

The FMR characterization was done using a vector network analyzer (VNA) and field-modulated (FM) FMR setup. The VNA-FMR was used to obtain  $S_{21}$  parameters from field-swept measurements as discussed by Kennewell *et al.*<sup>30</sup> It consisted of a Danphysik power supply to drive the electromagnets and an Agilent N5230 PNA-L vector network analyzer operating over a 1- to 20-GHz frequency range. The FM-FMR setup used the VNA as the microwave source and an SRS SR850 lock-in amplifier and HP 33120A function generator to drive the field-modulated measurements. Similar to the standard cavity FMR setup, an additional set of magnetic coils was used to modulate the applied field with an amplitude of 4–10 Oe and frequency of 220 Hz. The SR850 amplifier was locked to this frequency. In this arrangement, the output signal of the lock-in amplifier is proportional to the first derivative of the FMR absorption line with respect to the applied field. In both cases, a 0.3-mm-microstrip waveguide was used as the microwave antenna source as shown in Fig. 3. The sample was placed with the film in direct contact with the microstrip.

The in-plane FMR procedure for extracting resonance conditions was as follows. The frequency is constant, and an external magnetic field is swept while the  $S_{21}$  transmission coefficients are measured. This procedure was repeated for

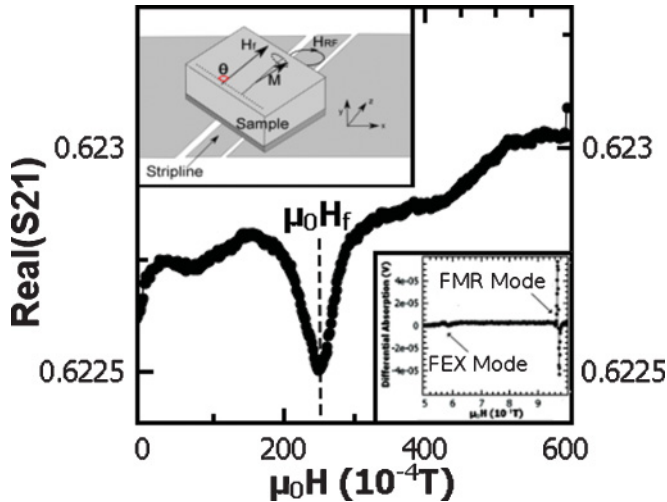


FIG. 3. (Color online) Raw data from the VNA-FMR sweep for the LSMO (38.86 nm) film in the  $0^\circ$  orientation with a 3-GHz driving microwave field. As the applied field is swept, the real part of the  $S_{21}$  parameter is measured [shown on the y axis as  $\text{Real}(S_{21})$ ], and when resonance occurs at  $H_f$ , there is a marked change in the  $\text{Real}(S_{21})$  coefficient. The top left inset displays a close picture of the in-plane experimental setup with the sample sitting on top of a strip line.  $M$  is the magnetization precessing in response to the driving microwave field  $H_{\text{rf}}$ , and the entire sample has its orientation varied by  $\theta$  with respect to the external field  $H_f$ . The bottom right inset displays a typical out-of-plane FM-FMR resonance experiment on the LSMO (54.8 nm) / BFO (23 nm) sample at a 14-GHz driving frequency. Both the FMR and FEX resonances are seen for this sample though the FEX mode has a much weaker resonance amplitude.

several different frequencies. An example result is shown in Fig. 3.

**V. FMR RESULTS AND DISCUSSION**

Only the FMR resonance was observed for the in-plane configuration. Lack of FEX mode absorption may correspond to weak surface pinning in the plane of the film. If surface pinning is weak, then the FEX mode has a symmetric magnetization profile across the film thickness, producing no net dipole moment to couple to.<sup>26</sup> In this case, only a nonuniform driving field, for example, caused by eddy currents in a conducting sample, can drive resonance.<sup>30-34</sup> However, we estimate that the nonuniformity of driving fields due to eddy currents are minimal given the conductivity of LSMO and the thicknesses of our samples. Hence, the FEX mode visibility should originate primarily from intrinsic surface pinning.

Magnetocrystalline anisotropies can be determined from angular measurements in plane as noted above. The results of an angular study of only the FMR mode are displayed in Fig. 4.

The type of anisotropy seems to be dependent on the film thickness. Films with the thinnest LSMO layer have a biaxial character while films with the thickest LSMO layer have a uniaxial character. There is also the case of the intermediate 45-nm LSMO film, which displays an unequal mixing of both

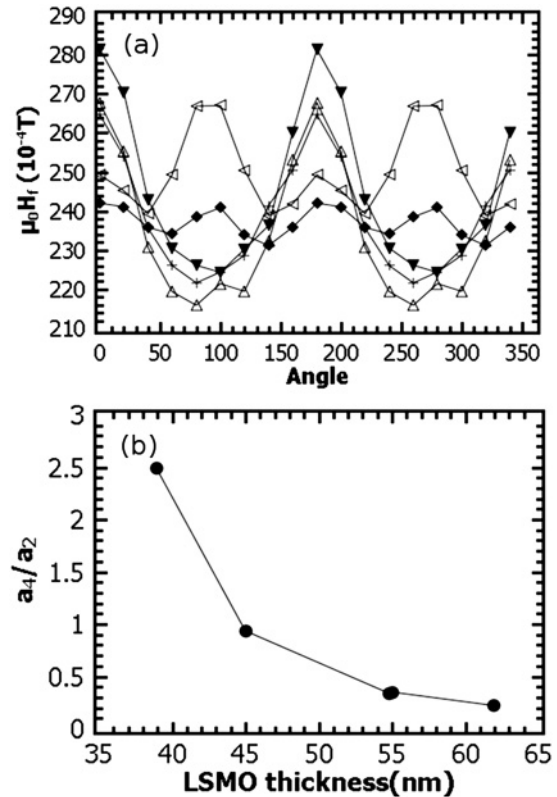


FIG. 4. (a) Resonant field  $H_f$  as a function of film angle  $\theta$ . All experiments used a 3-GHz driving microwave field: LSMO (38.89 nm) (solid diamond line), LSMO (45 nm) / PZT (20 nm) (empty sideways triangle line), LSMO (54.8 nm) / BFO (23 nm) (solid triangle line), LSMO (61.9 nm) (cross line), and LSMO (55 nm) / BFO (18 nm) (empty upright triangle line). The thinnest LSMO film clearly displays anisotropy of a biaxial character, whereas the thickest LSMO films have uniaxial characters. Interestingly, the 45-nm LSMO film displays a mixing of both anisotropy types. (b) The ratio of biaxial ( $a_4$ ) to uniaxial ( $a_2$ ) contributions from Eq. (3) vary with a  $1/t$  LSMO thickness dependence.

uniaxial and biaxial characters. Quantitative information on the form of the angular anisotropies can be obtained by fitting

$$H_f = a_0 + a_2 \sin(2\theta + \phi_1) + a_4 \sin(4\theta + \phi_2), \quad (3)$$

where  $H_f$  is the resonant applied field,  $\theta$  is the film angle with respect to the applied field,  $a_2$  is a uniaxial anisotropy term, and  $a_4$  is a biaxial anisotropy term. The  $\phi$ 's are phase shifts of the anisotropies with respect to the 0 measurement direction. Examining the ratio  $\frac{a_4}{a_2}$  as a function of LSMO thickness reveals a  $\frac{1}{t}$  trend as shown in Fig. 4, indicating that the uniaxial anisotropy dominates over the biaxial anisotropy as the LSMO thickness increases. Furthermore, this effect is related to the LSMO and substrate as it does not appear to be correlated with the capping layer.

Previous studies have noted both uniaxial and biaxial anisotropies present in STO/LSMO films with the biaxial anisotropy originating from the cubic symmetries of epitaxial LSMO grown on (001) STO and the uniaxial anisotropies originating from physical steps on the STO surface.<sup>13,35-37</sup> It has been reported that the in-plane fourfold and twofold

TABLE I. The extracted gyromagnetic ratio  $\gamma$  and effective internal field  $\mu_0 H_{\text{eff}}$  from data shown in Fig. 5. We attribute the distribution of  $\gamma$  to scatter in weak ferromagnetic resonance signals. Uncertainty in  $\mu_0 H_{\text{eff}}$  is  $\pm 50 \times 10^{-4}$  T and originates from the remanent magnetic field in our electromagnet pole pieces, the uncertainties in Hall probe calibration accuracy, and the imperfect line shapes of the FMR signal. Also, there are differences between the effective fields in the single-layer LSMO and capped LSMO films. In particular, films with a more positive  $\mu_0 H_{\text{eff}}$  must possess stronger out-of-plane bulk anisotropies or pinning. Differences in  $\mu_0 H_{\text{eff}}$  for the FMR and FEX modes demonstrate that interface pinning must play a role in these films. For empty entries, no FEX mode was observed.

Sample	$\gamma$ (FMR) $\times 10^{10}$ (Hz/T)	$\gamma$ (FEX) $\times 10^{10}$ (Hz/T)	$\mu_0 H_{\text{eff}}$ (FMR) (T)	$\mu_0 H_{\text{eff}}$ (FEX) (T)
STO / LSMO (30 nm)	2.79	2.79	-0.4425	-0.0956
STO / LSMO (38.9 nm)	2.67	2.67	-0.4624	-0.0973
STO / LSMO (61.9 nm)	2.83		-0.4891	
STO / LSMO (55 nm) / BFO (18 nm)	2.63		-0.4442	
STO / LSMO (54.8 nm) / BFO (24 nm)	2.64	2.64	-0.4423	-0.0437
STO / LSMO (45 nm) / PZT (20 nm)	2.63	2.63	-0.4089	0.0176

anisotropies are bulk in origin and not strongly related to interface pinning.

It should be noted, however, that both anisotropies are established during the growth process. In particular, because we measured a strong uniaxial anisotropy for 60-nm-thick single-layer LSMO films, it would seem unlikely that step defects<sup>38–40</sup> could explain these observations. The fact that this uniaxial anisotropy is dominant in thick LSMO films suggests that some kind of bulk structure first establishes at the step boundary and then propagates as the LSMO layer is grown.<sup>36</sup>

Each of the FMR angular resonance field plots in Fig. 4 has a different mean value constant offset, which does not depend on the LSMO thickness in a systematic way. The most likely explanation for this is either differences in saturation magnetization or pinning and out-of-plane anisotropy originating at the interface with the ferroelectric material. Without the additional FEX modes for the in-plane data, it is difficult to assess the contribution made by the ferroelectric layer to in-plane surface anisotropies.

FMR and FEX modes were seen for out-of-plane configuration measurements for some films. The films that do not have a number for  $H_{\text{eff}}$  (FEX) listed in Table I did not show the FEX mode. The FEX mode amplitude for all the samples which display it is about tenfold less than the fundamental mode (see the inset of Fig. 3 for a typical example). This amplitude level is close to the sensitivity threshold for the present experiment. The small amplitude of the FEX mode in Fig. 3 is consistent with it being the first-order standing spin wave mode that is made visible by asymmetric pinning. Since the pinning conditions and their symmetry are known to affect the FEX mode amplitude,<sup>41</sup> we speculate that the samples which do not display a FEX mode may have a slightly smaller or more symmetric magnetization surface or interface pinning. This results in a FEX amplitude below the threshold of sensitivity for the present experiment. Such variation in interface pinning may have origins in different interface terminations at the STO/LSMO and LSMO/BFO interfaces<sup>42</sup> or surface roughness at the LSMO/BFO interface. The lack of a FEX mode for all in-plane measurements and its presence in some out-of-plane resonance measurements indicate that surface pinning is most effective in the out-of-plane direction. When the surface pinning originates from an easy axis out-of-plane

anisotropy, it has been shown that both dynamic components of magnetization are pinned for the out-of-plane configuration but that only one component is pinned when the magnetization is in plane.<sup>43</sup> This may explain why these FEX modes are seen in out-of-plane resonance experiments and not in in-plane resonance experiments. As shown in Fig. 5, there is a strong FMR mode present in all films, and a FEX mode is observed in some films.

By fitting straight lines to the data in Fig. 5,  $\gamma$  and  $H_{\text{eff}}$  are extracted using Eq. (1). A comparison of these parameters for the different films is shown in Table I. The gyromagnetic ratio  $\gamma$  is extracted from the slope of the  $\omega(H_f)$  data given in Fig. 5.  $H_{\text{eff}}$  is measured by the intercept with  $\omega = 0$  for out-of-plane measurements. While the single-layer LSMO films show a net decrease in  $H_{\text{eff}}$  (FMR) with thickness, indicating a reduction

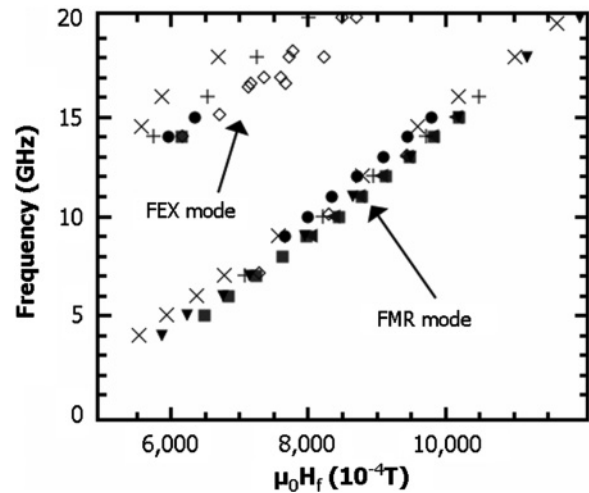


FIG. 5. Out-of-plane configuration resonant field  $H_f$  vs driving frequency  $\omega$  is shown for a variety of different films. LSMO (30 nm) (solid circles), LSMO (38.9 nm) (solid squares and empty diamonds), LSMO (61.9 nm) (solid sideways triangles), LSMO (55 nm) / BFO (17 nm) (solid down triangles), LSMO (54.8 nm) / BFO (24 nm) (plus symbols), and LSMO (45 nm) / PZT (20 nm) (cross symbols). One collection of data originates from the FMR mode (as shown), and the other collection of points are from the FEX mode. By fitting a linear function to these data, the gyromagnetic ratio  $\gamma$  and the effective internal field  $H_{\text{eff}}$  may be extracted.

TABLE II. Experimentally determined  $\mu_0\Delta H_{\text{eff}}$  are shown in the left column in units of Tesla and with an error of  $\pm 0.005$ . The right-hand column displays calculated  $\mu_0\Delta H_{\text{eff}}$  for the thicknesses of LSMO using the literature value of  $D_{\text{lit}} = 1.7965 \times 10^{-17} \text{ T m}^2$  and no interface pinning. Note that experimental  $\mu_0\Delta H_{\text{eff}}$  pinning from different capping layers appears significant.

	$\mu_0\Delta H_{\text{eff}}$ (experimental) (T)	$\mu_0\Delta H_{\text{eff}}$ (no pinning, $D_{\text{lit}}$ ) (T)
LSMO (30 nm)	0.3469	0.1970
LSMO (38.9 nm)	0.3651	0.1171
LSMO (45 nm) / PZT (20 nm)	0.4265	0.0875
LSMO (54.8 nm) / BFO (24 nm)	0.3986	0.0590

in out-of-plane anisotropies, the addition of a ferroelectric layer significantly changes  $H_{\text{eff}}$ . It should be noted that the PZT seems to have a greater influence on the magnetic parameters than BFO.

### VI. SPIN WAVE STIFFNESS

We now discuss the determination of  $D$  using the out-of-plane data. We define the gap between effective fields for the two modes  $\mu_0\Delta H_{\text{eff}}$  as

$$\begin{aligned} \mu_0\Delta H_{\text{eff}} &= \mu_0 H_{\text{eff}}(\text{FEX}) - \mu_0 H_{\text{eff}}(\text{FMR}) \\ &= D[k_{\text{oop}}^2(\text{FEX}) - k_{\text{oop}}^2(\text{FMR})]. \end{aligned} \quad (4)$$

Equation (4) does not contain contributions from  $\mu_0 M_S - \mu_0 H_{\text{oop}}$  as this contributes equally to both  $H_{\text{eff}}$  (FMR) and  $H_{\text{eff}}$  (FEX). Interface magnetization pinning will alter the wave number  $k$  of each mode by a different amount<sup>44</sup> so that different levels of pinning will result in a net change in  $\mu_0\Delta H_{\text{eff}}$ .

Table II lists the results of this gap for films in which the FEX mode was observed and also for estimates of what these values should be, assuming no interface pinning and a literature value of  $D_{\text{lit}} = 1.7965 \times 10^{-17} \text{ T m}^2$  (or in the units for exchange stiffness  $D_{\text{lit}} = 104 \text{ meV \AA}^2$ ). We note that the spin wave constant  $D$  used in the Kittel equation has units of Teslas per meter<sup>2</sup> and the spin wave stiffness  $D_{\text{stiffness}}$  is in units of Joules per meter<sup>2</sup>.<sup>11</sup> Assuming the average spin  $S = 1$ , conversion between the two uses the following:

$$D = \frac{D_{\text{stiffness}}}{\mu_B}.$$

It has been noted that  $S$  may have a range of values for Mn,<sup>45</sup> however determining  $S$  exactly is outside the scope of this study. There is a large discrepancy between the observed and predicted  $\mu_0\Delta H_{\text{eff}}$  values. As surface pinning may be equally likely from both the substrate and the ferroelectric

material, we thus consider two extreme situations to account for the observed  $\mu_0\Delta H_{\text{eff}}$ : complete pinning at the ferroelectric interface only (single-sided pinning) and complete pinning at both interfaces (double-sided pinning).<sup>46</sup> Theoretically calculated values for  $\mu_0\Delta H_{\text{eff}}$  gaps in a 38.9-nm LSMO film for extreme pinning conditions are given in Table III. The case where  $D = D_{\text{lit}}$  accounts for  $\mu_0\Delta H_{\text{eff}}$  values seen in experiments can occur for only double-sided pinning. In the case where extreme single-sided magnetization pinning exists, an exchange constant value of at least  $D = 1.56 \times D_{\text{lit}}$  is needed. Finally, the case where  $\mu_0\Delta H_{\text{eff}}$  can be explained without any interface pinning is possible for only  $D = 3.12 \times D_{\text{lit}}$ . Unless extreme double-sided pinning exists for the STO/LSMO, then the exchange constant  $D$  is larger than commonly found in the literature. In addition, there is a greater  $\mu_0\Delta H_{\text{eff}}$  gap for the films with a capping ferroelectric material, especially for the PZT-capped films, indicating out-of-plane interface pinning which originates from the ferroelectric layer.

### VII. SUMMARY

Ferromagnetic resonance was used as a sensitive probe of both in-plane and out-of-plane anisotropies in multilayer LSMO/BFO and LSMO/PZT films. We have shown that some interface pinning must play a role in magnetization dynamics. Interestingly, BFO seems to have little influence on the bulk magnetization of LSMO. We see no evidence of exchange bias,<sup>5,6</sup> though this may be because of the relatively thick LSMO layer dominating the magnetization dynamics. The slow growth rate of our BFO in comparison to the BFO growth rate used by Martin *et al.*<sup>5</sup> to produce exchange biasing effects may also be an important factor in growing suitable BFOs to couple to the ferromagnets. Electric fields were applied across the BFO layer, and resonance experiments were carried out, but no shifts in FMR resonances were observed. From our data, it is quite difficult to extract separate pinning effects at

TABLE III. Theoretically calculated  $\mu_0\Delta H_{\text{eff}}$  (in Teslas) for a 38.9-nm LSMO film given various extreme interface pinning conditions (top row) and different values of  $D$  (with respect to  $D_{\text{lit}} = 1.7965 \times 10^{-17} \text{ T m}^2$ ). It is important to note the experimental  $\mu_0\Delta H_{\text{eff}} = 0.3651 \text{ T}$ . Assuming that the entirety of pinning originates from one interface,  $D = 1.56D_{\text{lit}}$  in order to match the theoretically predicted effective field gap to the experimentally determined one as indicated in the table.

	No pinning (T)	Max single-sided pinning (T)	Max double-sided pinning (T)
$D_{\text{lit}}$	0.1171	0.2343	0.3515
$1.56D_{\text{lit}}$	0.1828	0.3656	0.5484
$3.12D_{\text{lit}}$	0.3656	0.7311	1.0967

each interface. However, a lower bound for  $D$  can be set, given various assumptions about pinning at the interface. We found that complete pinning at both interfaces gives the same value of  $D$  for our films as that of  $D_{\text{fit}}$ .

Uniaxial and biaxial in-plane anisotropies which appear to be unrelated to the capping ferroelectric layer were observed, and there may exist a thickness of LSMO about which a transition between anisotropies might take place. Our data indicate that the uniaxial contribution to the anisotropy

relative to the biaxial component increases as the ferromagnet thickness increases for LSMO films grown on STO(100), unlike that found for LSMO grown on other substrates.<sup>8</sup>

#### ACKNOWLEDGMENTS

We acknowledge the support of the ARC, University of Western Australia, DEST, and the DIISR Australia-India Strategic Research Fund (Grant No. ST020078).

\*rhet.magaraggia@gmail.com

<sup>1</sup>Z. Shi, C. Wang, X. Liu, and C. Nan, *Chin. Sci. Bull.* **53**, 2135 (2008).

<sup>2</sup>S. Majumdar, R. Laiho, P. Laukkanen, I. J. Väyrynen, H. S. Majumdar, and R. Österbacka, *Appl. Phys. Lett.* **89**, 122114 (2006).

<sup>3</sup>F. J. Wang, C. G. Yang, Z. V. Vardeny, and X. G. Li, *Phys. Rev. B* **75**, 245324 (2007).

<sup>4</sup>J.-H. Park, E. Vescovo, H. J. Kim, C. Kwon, R. Ramesh, and T. Venkatesan, *Nature (London)* **392**, 794 (1998).

<sup>5</sup>L. W. Martin, Y.-H. Chu, M. B. Holcomb, M. Huijben, P. Yu, S.-J. Han, D. Lee, S. X. Wang, and R. Ramesh, *Nano Lett.* **8**, 2050 (2008).

<sup>6</sup>J. Dho, X. Qi, H. Kim, J. MacManus-Driscoll, and M. Blamire, *Adv. Mater.* **18**, 1445 (2006).

<sup>7</sup>S. M. Wu, S. A. Cybart, P. Yu, M. D. Rossell, J. X. Zhang, R. Ramesh, and R. C. Dynes, *Nat. Mater.* **9**, 756 (2010).

<sup>8</sup>H. Nishikawa, E. Houwman, H. Boschker, M. Mathews, D. H. A. Blank, and G. Rijnders, *Appl. Phys. Lett.* **94**, 042502 (2009).

<sup>9</sup>I. Gomes, B. Almeida, A. Lopes, J. Araújo, J. Barbosa, and J. Mendes, *J. Magn. Magn. Mater.* **322**, 1174 (2010).

<sup>10</sup>M. Huijben, L. W. Martin, Y.-H. Chu, M. B. Holcomb, P. Yu, G. Rijnders, D. H. A. Blank, and R. Ramesh, *Phys. Rev. B* **78**, 094413 (2008).

<sup>11</sup>M. Golosovsky, P. Monod, P. K. Muduli, and R. C. Budhani, *Phys. Rev. B* **76**, 184413 (2007).

<sup>12</sup>A. A. Sidorenko, G. Allodi, R. De Renzi, G. Balestrino, and M. Angeloni, *Phys. Rev. B* **73**, 054406 (2006).

<sup>13</sup>Y. Suzuki, H. Y. Hwang, S.-W. Cheong, and R. B. van Dover, *Appl. Phys. Lett.* **71**, 140 (1997).

<sup>14</sup>S. E. Lofland, S. M. Bhagat, Q. Q. Shu, M. C. Robson, and R. Ramesh, *Appl. Phys. Lett.* **75**, 1947 (1999).

<sup>15</sup>J. Dho and N. Hur, *J. Magn. Magn. Mater.* **318**, 23 (2007).

<sup>16</sup>L. B. Steren, M. Sirena, and J. Guimpel, *J. Appl. Phys.* **87**, 6755 (2000).

<sup>17</sup>M. Ziese, I. Vrejoiu, E. Pippel, P. Esquinazi, D. Hesse, C. Etz, J. Henk, A. Ernst, I. V. Maznichenko, W. Hergert, and I. Mertig, *Phys. Rev. Lett.* **104**, 167203 (2010).

<sup>18</sup>C. Thiele, K. Dörr, S. Fähler, L. Schultz, D. C. Meyer, A. A. Levin, and P. Paufler, *Appl. Phys. Lett.* **87**, 262502 (2005).

<sup>19</sup>M. C. Martin, G. Shirane, Y. Endoh, K. Hirota, Y. Moritomo, and Y. Tokura, *Phys. Rev. B* **53**, 14285 (1996).

<sup>20</sup>L. Vasiliu-Doloc, J. W. Lynn, Y. M. Mukovskii, A. A. Arsenov, and D. A. Shulyatev, *J. Appl. Phys.* **83**, 7342 (1998).

<sup>21</sup>A. H. Moudden, L. Vasiliu-Doloc, L. Pinsard, and A. Revcolevschi, *Physica B* **241-243**, 276 (1997).

<sup>22</sup>W. Stoecklein, S. S. P. Parkin, and J. C. Scott, *Phys. Rev. B* **38**, 6847 (1988).

<sup>23</sup>R. D. McMichael, M. D. Stiles, P. J. Chen, and W. F. Egelhoff, *Phys. Rev. B* **58**, 8605 (1998).

<sup>24</sup>B. K. Kuanr, S. Maat, S. Chandrashekariiah, V. Veerakumar, R. E. Camley, and Z. Celinski, *J. Appl. Phys.* **103**, 07C107 (2008).

<sup>25</sup>C. Kittel, in *Introduction to Solid State Physics*, 8th ed., edited by S. Johnson (John Wiley & Sons, New York, 2005).

<sup>26</sup>C. Kittel, *Phys. Rev.* **110**, 1295 (1958).

<sup>27</sup>J. M. H. Seavey and P. Tannenwald, *Phys. Rev. Lett.* **1**, 168 (1958).

<sup>28</sup>R. L. Stamps, R. E. Camley, and R. J. Hicken, *Phys. Rev. B* **54**, 4159 (1996).

<sup>29</sup>M. Hambe, A. Petraru, N. A. Pertsev, P. Munrow, V. Nagarajan, and H. Kohlstedt, *Adv. Funct. Mater.* **20**, 2436 (2010).

<sup>30</sup>K. J. Kennewell, M. Kostylev, N. Ross, R. Magaraggia, R. L. Stamps, M. Ali, A. A. Stashkevich, D. Greig, and B. J. Hickey, *J. Appl. Phys.* **108**, 073917 (2010).

<sup>31</sup>M. Kostylev, *J. Appl. Phys.* **106**, 043903 (2009).

<sup>32</sup>W. S. Ament and G. T. Rado, *Phys. Rev.* **97**, 1558 (1955).

<sup>33</sup>Y. V. Khivintsev, L. Reisman, J. Lovejoy, R. Adam, C. M. Schneider, R. E. Camley, and Z. J. Celinski, *J. Appl. Phys.* **108**, 023907 (2010).

<sup>34</sup>P. Pincus, *Phys. Rev.* **118**, 658 (1960).

<sup>35</sup>M. Mathews, F. M. Postma, J. C. Lodder, R. Jansen, G. Rijnders, and D. H. A. Blank, *Appl. Phys. Lett.* **87**, 242507 (2005).

<sup>36</sup>Z. H. Wang, G. Cristiani, and H. U. Habermeier, *Appl. Phys. Lett.* **82**, 3731 (2003).

<sup>37</sup>P. Perna, C. Rodrigo, E. Jiménez, F. J. Teran, N. Mikuszeit, L. Méchin, J. Camarero, and R. Miranda, *J. Appl. Phys.* **110**, 013919 (2011).

<sup>38</sup>R. Arias and D. L. Mills, *Phys. Rev. B* **59**, 11871 (1999).

<sup>39</sup>D. S. Chuang, C. A. Ballentine, and R. C. O'Handley, *Phys. Rev. B* **49**, 15084 (1994).

<sup>40</sup>L. Néel, *J. Phys. Radium* **15**, 225 (1954).

<sup>41</sup>A. G. Gurevich and G. A. Melkov, *Magnetization Oscillations and Waves* (CRC Press, Boca Raton, FL, 1996).

<sup>42</sup>H. Zenia, G. A. Gehring, and W. M. Temmerman, *New J. Phys.* **9**, 105 (2007).

<sup>43</sup>N. Salansky and M. Erukhimov, *Physical Properties and Application of Magnetic Films* (Nauka, Moscow, 1975).

<sup>44</sup>R. Magaraggia, K. Kennewell, M. Kostylev, R. L. Stamps, M. Ali, D. Greig, B. J. Hickey, and C. H. Marrows, *Phys. Rev. B* **83**, 054405 (2011).

<sup>45</sup>M. Sikora, K. Knizek, Cz. Kapusta, and P. Glatzel, *J. Appl. Phys.* **103**, 07C907 (2008).

<sup>46</sup>We note that if complete pinning does occur at both interfaces, then the first exchange mode becomes symmetric and will not be excited by a uniform driving field. In our experiment, only the conductivity would cause a nonuniform driving field [31], and this effect is estimated to be quite weak for LSMO. Hence, a first exchange mode which experiences double-sided pinning would be extremely difficult to detect. In our estimation of the theoretical range of  $D$ , we neglect this fact.